Plasmonic Monitoring of Catalytic Hydrogen Generation by a Single Nanoparticle Probe

3 AUTHORS, INCLUDING:

Daeha Seo

University of California, San Francisco

21 PUBLICATIONS **830** CITATIONS

Plasmonic Monitoring of Catalytic Hydrogen Generation by a Single Nanoparticle Probe

Daeha Seo, Garam Park, and Hyunjoon Song*

Department of Chemistry, Korea Advanced Institute of Science and Technology, Daejeon 305-701, Korea

ⓢ Supporting Information

ABSTRACT: Plasmonic nanostructures such as gold nanoparticles are very useful for monitoring chemical reactions because their optical properties are highly dependent upon the environment surrounding the particle surface. Here, we designed the catalytic structure composed of platinized cadmium sulfide with gold domains as a sensitive probe, and we monitored the photocatalytic decomposition of lactic acid to generate hydrogen gas in situ by single-particle dark-field spectroscopy. The plasmon band shift of the gold probe throughout the reaction exhibits significant particle-to-particle variation, and by simulating the reaction kinetics, the rate constant and structural information (including the diffusion coefficient through the shell and the relative arrangement of the active sites) can be estimated for individual catalyst particles. This approach is versatile for the monitoring of various heterogeneous reactions with distinct components at a single-particle level.
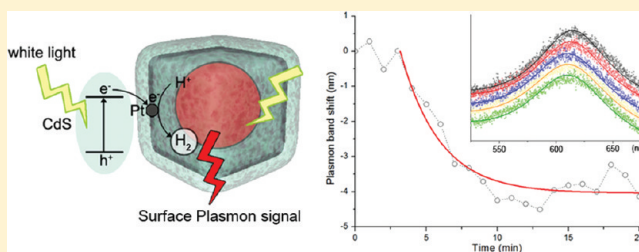
INTRODUCTION

Heterogeneous catalysts have been widely used in various chemical transformations from the synthesis of chemical resources and pollutant removal to electrochemical cells for energy conversion. Heterogeneous catalytic systems are rather sophisticated because the associated reactions mainly occur at the interface between multiple phases, where the solid surface provides active reaction sites. Numerous catalytic factors influence the reaction rates, including the surface facets, the active surface atoms at edges and kinks, and the atomic arrangement, as well as the average surface area and composition.[1−6] To simplify the reaction system, solid substrates with single-crystalline faces have been employed as model catalysts to investigate surface-dependent reaction properties.[7−10] Recently, the model catalysts have been extended to three-dimensional structures bearing metal nanoparticles and have provided valuable information regarding actual catalytic reactions.[11] However, these approaches have fundamental limitations due to ensemble average measurements because the individual catalyst particles have broad distributions of particle size and reaction environment. Another serious challenge is in situ reaction monitoring during the reaction process. For the detection of intermediate stages, the reactions have been investigated using special surface techniques, which usually require high-vacuum conditions with powerful irradiation of light or subatomic particles, producing situations that are far from the real reaction conditions.[8−10]

Surface plasmon resonance (SPR) is a phenomenon involving the coupling of irradiated light and conducting electrons. It leads to intense light scattering, which is highly dependent upon the dielectric constants of the surrounding media.[12] Accordingly, it is useful in monitoring changes in the surfaces of metallic nanostructures. Anker et al. employed SPR for highly sensitive chemical and biomolecular detection,[13] and Larsson et al. used it to continuously monitor gas-phase reactions.[14] These plasmon-based techniques are advantageous in terms of real-time, label-free, and high-resolution sensing without requiring special treatment of the specimen.

Recent developments in surface plasmon measurement have made it possible to study chemical properties at a single-particle level. Novo et al. and Xu et al. reported the direct observation of chemical reactions on individual gold nanocrystal surfaces.[15,16] The optical property of single gold nanorods was modulated by electrochemical charge injection, which would guide the redox reaction mechanisms at the level of single electrons.[17] Hydrogen adsorption and desorption on individual Pd nanoparticles were also detected by introducing plasmonic gold nanostructures.[18,19]

In the present study, we introduced gold probes into a heterogeneous catalytic system and monitored the reaction progress in situ by single-particle dark-field spectroscopy. Specially designed catalytic structures bearing the gold probes carried out the hydrogen generation reaction, and the SPR peak change provided critical information regarding individual particle properties, such as reaction kinetics and the geometry of individual catalytic nanoparticles.
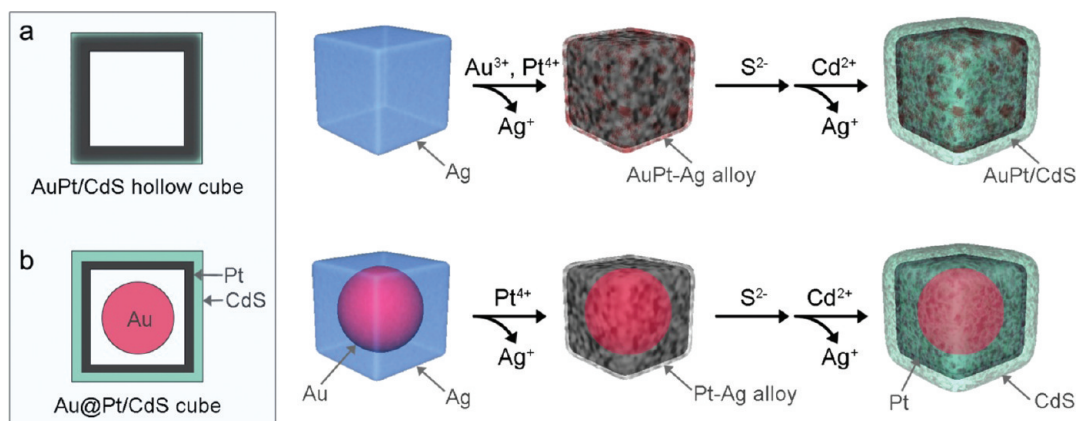
EXPERIMENTAL SECTION

Synthesis of AuPt/CdS Hollow Cubes. Silver cubes were synthesized via the polyol process developed by Zhang et al.[20] First,

Figure 1. Structural design and synthetic scheme of catalytic particles bearing gold probes: (a) AuPt/CdS hollow cubes; (b) Au@Pt/CdS cubes.

a silver cube dispersion in ethanol (2.6 mL, 0.19 mmol with respect to the original silver precursor concentration) was added to a boiling aqueous solution of PVP (M_w = 55 000, 50 mL, 0.60 mmol). Next, $HAuCl_4$ (10 mL, 0.016 mmol) and H_2PtCl_6 (10 mL, 0.011 mmol) aqueous solutions were added dropwise to the boiling mixture for 7 min, followed by reflux for another 3 min. After centrifugation, the resultant AuPt−Ag hollow cubes were dispersed in water (30 mL).

Second, the aqueous dispersion of the AuPt−Ag hollow cubes (26 mL) and PVP (0.049 g, 0.44 mmol) was added to water (200 mL). The Na_2S aqueous solution (8.9 mL, 10 mM) was added, and the reaction mixture was allowed to stir for 1 d. After centrifugation, the resultant $AuPt/Ag_2S$ hollow cubes were dispersed in methanol (10 mL).

Third, the methanol dispersion of the $AuPt/Ag_2S$ hollow cubes (9.0 mL), $Cd(NO_3)_2$ solution in methanol (8.0 mL, 8.0 mmol), and tributylphosphine (TBP, 2.2 mL, 9.9 mmol) was added to methanol (40 mL), and the reaction mixture was stirred for 3 d. After centrifugation, the resultant AuPt/CdS hollow cubes were dispersed in methanol (5.0 mL).

Synthesis of Au@Pt/CdS Cubes. Au@Ag core−shell cubes were synthesized via the seed-mediated polyol process developed by Park et al.[21] First, the Au@Ag core−shell cube dispersion in ethanol (5.0 mL, 0.076 and 0.53 mmol with respect to the original gold and silver precursor concentrations, respectively) was added to the boiling aqueous solution of PVP (100 mL, 0.31 mmol). Next, the H_2PtCl_6 (12 mL, 0.0056 mmol) aqueous solution was added dropwise to the boiling mixture for 3 min, followed by reflux for another 3 min. After centrifugation, the resultant Au@Pt−Ag cubes were dispersed in water (10 mL).

Second, PVP (0.017 g, 0.15 mmol) was added to the aqueous dispersion of the Au@Pt−Ag cubes (5.0 mL). The Na_2S aqueous solution (2.2 mL, 10 mM) was added, and the reaction mixture was allowed to stir for 1 d. After centrifugation, the resultant $Au@Pt/Ag_2S$ cubes were dispersed in methanol (10 mL).

Third, the $Cd(NO_3)_2$ solution in methanol (1.3 mL, 1.3 mmol) and TBP (0.37 mL, 1.7 mmol) was added to the methanol dispersion of the $Au@Pt/Ag_2S$ cubes (3.0 mL), and the reaction mixture was allowed to stir for 3 d. After centrifugation, the resultant Au@Pt/CdS cubes were dispersed in methanol (5.0 mL).

Monitoring Photocatalytic Decomposition of Lactic Acid. Glass slides and coverslips were cleaned using aqua regia and piranha solutions, and ultimately a large amount of distilled water. The reaction chamber was formed using double-sided tape on the glass slide. The highly diluted catalyst dispersion (∼1/1000 dilution of the original dispersion with methanol) was cast onto the glass slide, and the sample was allowed to dry for 1 min. For the reaction, 10% lactic acid was added onto the reaction chamber. A coverslip covered the chamber.

Dark-field scattering measurements were performed with an inverted microscope (Carl Zeizz, Axiovert 40). The sample was illuminated by a halogen lamp (35 W) using a dark-field condenser

(N.A. = 1.3) with immersion oil. Light was collected through a 43× microscope objective lens (N.A. = 0.98) and captured by a 640 × 480 pixel color video camera (SONY, SSC-DC80) for images and a CCD camera (ANDOR, NEWTON DU971N) with monochromator (Dongwoo, 500i) for spectra. The extinction spectrum was integrated for 45 s and was extracted by background subtraction and lamp spectrum correction.

■ RESULTS AND DISCUSSION

To demonstrate, we chose the photocatalytic decomposition of lactic acid on platinized cadmium sulfide (Pt/CdS), which yields pyruvic acid and hydrogen gas.[22] The Pt/CdS system is known to efficiently decompose organic molecules due to the large bandgap of CdS (2.410 eV). The reaction was expected to cause a large change in the refractive index (n) between the reactants (1.425 for lactic acid) and the products (1.416 for pyruvic acid and 1.000 for H_2 gas). If the catalyst structure is a hollow shell with the active sites located inside, the reaction mainly occurs on the internal surface, and hydrogen gas should accumulate in the vacancy.

To effectively probe the reaction, we introduced Au(0) domains into the catalyst structure in two ways. The first was to locate the Au domains in close proximity to the active Pt sites to detect hydrogen evolution directly (Figure 1a). In this arrangement, the reaction progress can be monitored from very early moments, but the Au domains may interact electronically with the active Pt sites and affect catalytic behaviors. The second way to detect hydrogen evolution is to separate the Au domains by some distance from the Pt sites to observe the actual reaction progress on the Pt/CdS catalyst surface without any interference (Figure 1b). These two distinct catalyst designs are referred to as AuPt/CdS hollow cubes and Au@Pt/CdS cubes, respectively.

The catalysts were synthesized via three steps. For the former structure, partial galvanic replacement of the silver cubes[20] with platinum and gold precursors yielded AuPt−Ag alloy hollow cubes. Subsequent chalcogenization with S^{2-} and cationic exchange with Cd^{2+} yielded AuPt/CdS hollow cubes. Scanning electron microscopy (SEM), high-angle annular dark-field-scanning electron microscopy (HAADF-STEM), high-resolution transmission electron microscopy (HRTEM), and X-ray diffraction (XRD) data show that the structures are completely converted from silver cubes to AuPt−Ag alloy hollow cubes, $AuPt/Ag_2S$ hollow cubes, and eventually AuPt/CdS hollow cubes, respectively, with the preservation of the cubic frameworks (Supporting Information, Figures S1−S3, and
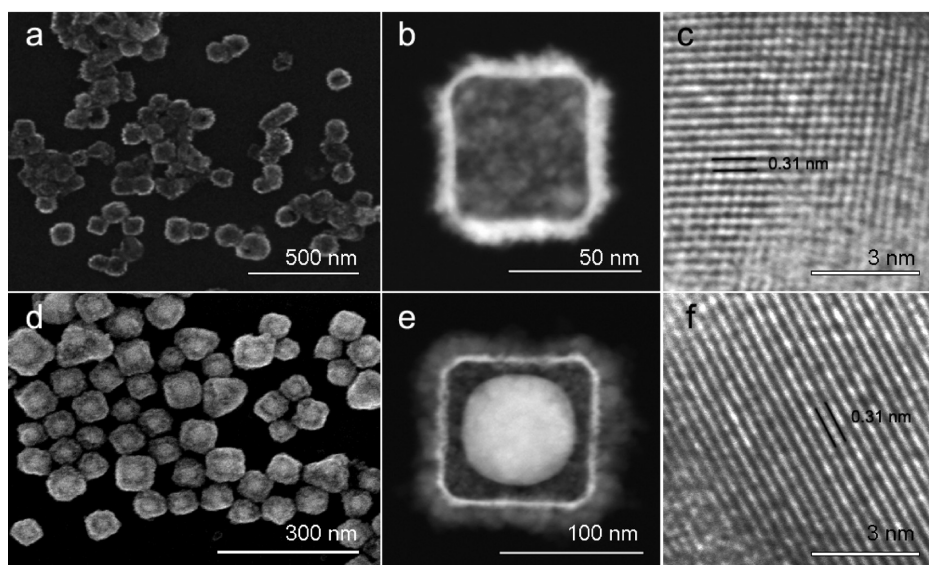
Figure 2. Electron microscopy images of catalytic particles. SEM, HAADF-STEM, and HRTEM images of (a−c) AuPt/CdS hollow cubes, and (d−f) Au@Pt/CdS cubes.

Figure 2a−c). The resultant AuPt/CdS hollow cubes have an average edge size of 66 ± 10 nm with an average wall thickness of 10 ± 3 nm. Individual hollow cubes have a rough surface with coarse domains (Figure 2b). The HRTEM image shows that the particles possess polycrystalline nature with single-crystal domains of CdS (Figure 2c). The elemental mapping image indicates that Au, Pt, S, and Cd components are distributed evenly over the hollow structure (Supporting Information, Figure S4). The energy dispersive X-ray spectroscopy (EDS) data show that some compositional variations of Pt and Au exist in individual particles, although the total atomic % of Pt and Au is invariable (Supporting Information, Figure S5).

By contrast, the Au@Pt/CdS cubes are relatively uniform both in shape and in composition. The partial galvanic replacement reaction of Au@Ag core−shell cubes[21] with the Pt precursor yielded Au@Pt−Ag alloy hollow cubes, and chalcogenization with $S^{2−}$ and cationic exchange with Cd^{2+} afforded Au@Pt/CdS cubes. A series of characterization results prove the complete conversion from the Au@Ag core−shell cubes to the final Au@Pt/CdS cubes, respectively (Supporting Information Figures S6−S8, and Figure 2d−f). The resulting Au@Pt/CdS cubes have an average edge size of 140 ± 20 nm with the average wall thickness of 20 ± 4 nm. The average diameter of the Au cores is estimated to be 60 ± 11 nm. On the basis of the SEM image and EDS analysis, each nanocube is observed to comprise double layers of inner Pt and outer CdS shells with a spherical Au core at the center. The double layers of Pt and CdS are also distinct in the elemental mapping data (Supporting Information Figures S9, S10). The outermost CdS layers have large single-crystalline domains with a distance of 0.31 nm between the neighboring lattice fringe images, corresponding to that of monoclinic CdS(101) (Figure 2f). Such clear separation of the Pt and CdS layers is mainly attributed to a combination of galvanic replacement and the Kirkendall effect during the sulfidation reaction. The partial galvanic replacement reaction yielded Pt layers located at the faces of the original silver cubes. The remaining Ag(0) components of the Pt−Ag alloy hollows reacted with $S^{2−}$ to form Ag_2S shells outside the Pt layers. The double-shell formation is elucidated by the nanoscale Kirkendall effect,[23] in

which the difference in the diffusion coefficients of Ag (D_{Ag} = 9.981×10^{-2} cm^2 s^{-1} at 298 K) and S ($D_S = 1.901 \times 10^{-2}$ cm^2 s^{-1} at 298 K)[24] across the Pt layers leads to a net Ag flow outward and an opposite flow of vacancies inward, forming a hollow shell structure. The ensuing cation exchange converted the Ag_2S into the CdS shells outside the Pt layers distinctively. In the AuPt/CdS hollow cubes, such distinctive layer formation was not observed, presumably because of the coarse deposition of Pt and Au together on the original silver cube surface during the partial galvanic replacement.

The optical properties of the catalyst particles were measured both in bulk aqueous dispersions (n = 1.333) by UV−vis spectroscopy and in individual particles immersed in an emersion oil (n = 1.515) by dark-field spectroscopy. The bulk spectrum of the AuPt/CdS hollow cubes has a broad peak at a maximum of 550 nm, while the single-particle signal appears at 575 nm, which are consistent with each other considering the surrounding media (Supporting Information, Figure S11). The extinction peaks of the Au@Pt/CdS cubes appear at 485 and 590 nm (Figure 3a, black). The former can be assigned to that of the Pt/CdS hollow shells, by confirming
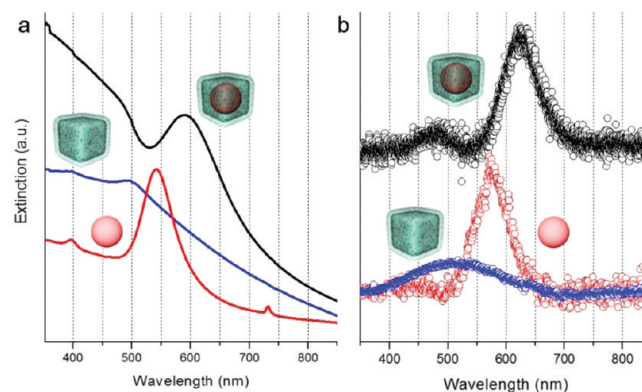
Figure 3. Optical properties of Au@Pt/CdS cubes. (a) UV−vis and (b) single-particle dark-field spectra of free-standing Au spheres (red), Pt/CdS hollow cubes (blue), and Au@Pt/CdS cubes (black).
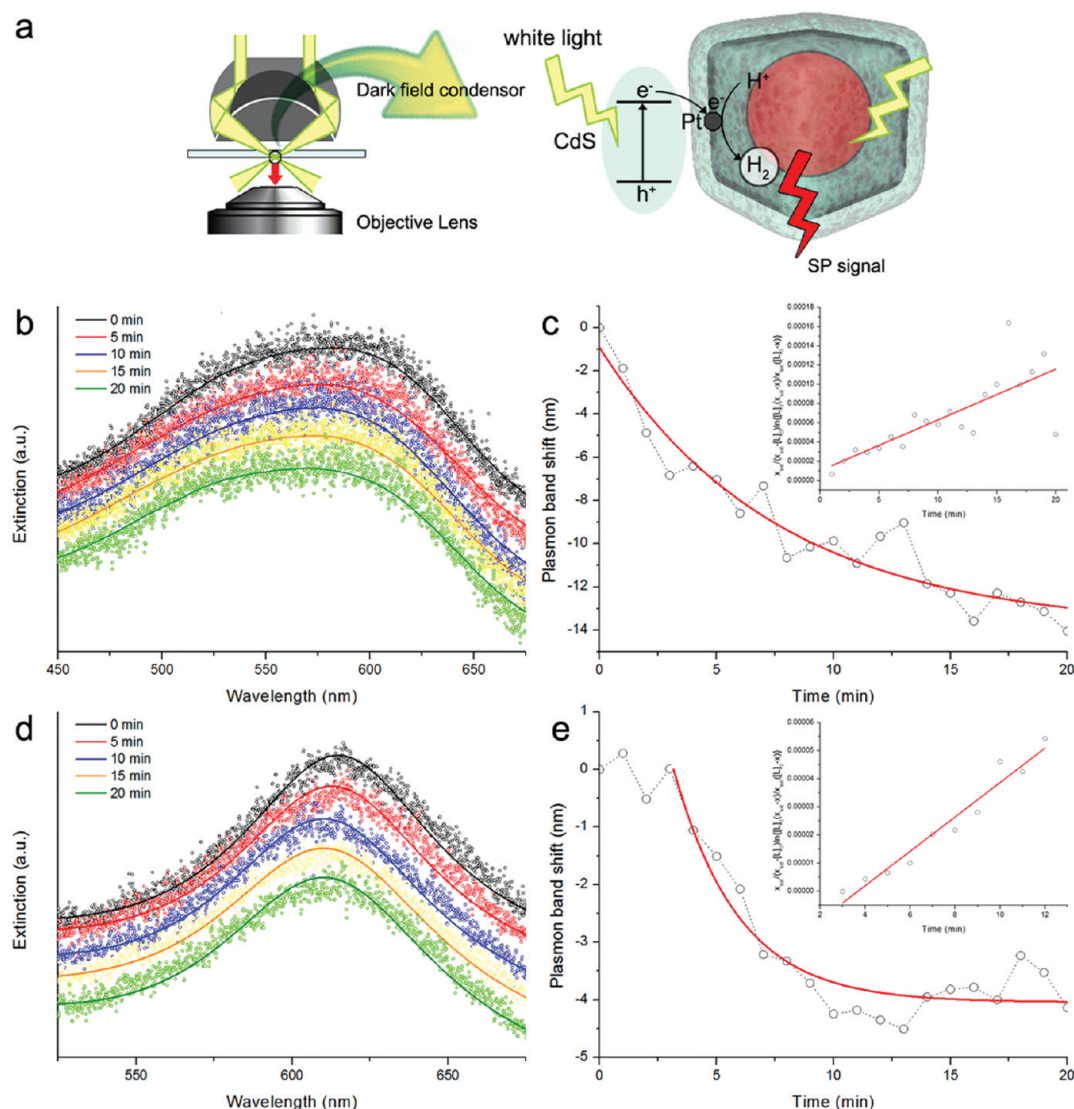
Figure 4. Monitoring of hydrogen evolution by single-particle dark-field spectroscopy. (a) Schematic diagram of single-particle measurement and detection on a single Au@Pt/CdS catalyst particle. (b) Extinction spectra and (c) plasmon band shifts of a single AuPt/CdS hollow cube along the reaction progress. (d) Extinction spectra and (e) plasmon band shifts of a single Au@Pt/CdS cube along the reaction progress. (c and e insets) Kinetic plots along the reaction progress based on eq 1.

the peak at 490 nm of the Pt/CdS hollow particles (blue) that are directly synthesized from the silver cubes. The 590 nm peak is the extinction of the Au cores, which is significantly red-shifted as compared to that of the free-standing Au spheres with identical diameters (542 nm, red). A similar peak shift is observed in the single-particle dark-field spectra (Figure 3b). The spectrum of a single particle exhibits a broad peak at 474 nm arising from the Pt/CdS hollow shell (blue), and a sharp peak at 629 nm assignable to that of the Au core. A red-shift of 52 nm from the peak of a free-standing Au sphere (577 nm, red) is ascribed to the plasmon coupling of the Au core and the Pt/CdS hollow shell.[25,26]

To check the relationship between the refractive index of surrounding medium (n) and the maximum plasmon peak shift ($\Delta\lambda$),[12] the catalyst particles were immersed in four different media, air, water, ethylene glycol ($n = 1.438$), and immersion oil, respectively, and the maximum extinction peaks were measured (Supporting Information, Figure S12). From the slopes of the linear fits, the sensitivity factors, $\Delta\lambda/\Delta n$, were estimated to be 34.5 nm RIU^{-1} for the AuPt/CdS hollow cubes

and 32.9 nm RIU^{-1} for the Au@Pt/CdS cubes, respectively. Such low sensitivity factors as compared to those ($\sim$60 nm RIU^{-1}) of Au nanoparticles[27] are due to the existence of other components such as Pt and CdS around the Au probes.

On the basis of these optical properties, the two different catalysts were employed for hydrogen gas evolution by the photocatalytic decomposition of lactic acid, and the reactions were monitored by single-particle dark-field spectroscopy. Under white-light irradiation with a halogen lamp (35 W) through a dark-field condenser (N.A. = 1.3), photons coincident with the band gap are absorbed in the CdS shells to generate photoelectrons, which transfer to the Pt sites, and react with protons in solution to generate hydrogen gas. The operational model of dark-field spectroscopy and the detection scheme on a single particle are depicted in Figure 4a.

At $t = 0$, 10% lactic acid solution in water was introduced as a proton source, and the plasmon scattering signal of an individual particle was measured every minute. Figure 4b shows the extinction peak change of a single AuPt/CdS hollow cube during the reaction. The plasmon band at 569 nm

Table 1. Estimation of Rate Constant (k), Diffusion Coefficient (D), and Pt–Au Distance (d) of 10 Individual (a) AuPt/CdS Hollow Cubes and (b) Au@Pt/CdS Cubes

		(a) Individual AuPt/CdS Hollow Cubes		
particle no.	peak shift (nm)	rate constant k (10^{-6} M^{-1} min^{-1})	reverse peak shift (nm)	diffusion coefficient D (10^{-19} m^2 s^{-1})
1	−16.7	5.8		
2	−14.6	14.2	5.2	3.7
3	−10.4	9.9	7.4	1.2
4	−18.5	9.0		
5	−9.4	9.3		
6	−6.3	7.2		
7	−14.0	5.3		
8	−8.1	17.3		
9	−6.8	7.6	2.9	2.8
10	−11.8	4.1		
average	−10.7 ± 4.1	9.5 ± 4.5		

			(b) Individual Au@Pt/CdS Cubes			
particle no.	peak shift (nm)	rate constant k (10^{-6} M^{-1} min^{-1})	reverse peak shift (nm)	diffusion coefficient D (10^{-19} m^2 s^{-1})	delay time (s)	Pt–Au distance d (nm)
1′	−4.5	6.1			3	17.8
2′	−5.5	8.4	2.4	1.8	8	25.3
3′	−2.9	4.8	2.2	2.1	3	17.2
4′	−3.9	4.1			3	16.9
5′	−4.6	2.6			4	16.6
6′	−2.8	2.7			10	19.2
7′	−8.1	6.8			2	17.1
8′	−3.3	2.2	1.8	1.2	4	16.3
9′	−4.8	12.8			12	38.6
10′	−3.9	4.6	2.7	2.9	4	17.8
average	−4.4 ± 1.5	6.5 ± 3.2			5 ± 3	20.3 ± 7.0

gradually shifts to a shorter wavelength, and the maximum peak shift ($\Delta\lambda_{max}$) is −14 nm during the reaction. If the environment around the Au probe is completely converted from the reactant solution (10% lactic acid in water, $n = 1.342$) to hydrogen gas ($n = 1.000$), the plasmon band shift is estimated to be −12 nm by Mie theory, indicating that our measurement is reasonable within the error range. In a control experiment, the present reaction conditions in the absence of lactic acid did not exhibit any plasmon shifts during the reaction period (Supporting Information, Figure S13), which excludes the possibility of plasmon frequency change by photoelectron injection from CdS ($\omega_p^2 = de^2/m_{eff}\varepsilon_0$, where ω_p is plasmon frequency, d is electron density, e is electron charge, m_{eff} is effective mass of the electron, and ε_0 is vacuum permittivity).[28] After the irradiation, the catalyst particle showed a peak shift pattern similar to that of the fresh catalyst, indicating high stability of the catalyst against photocorrosion.[22]

Figure 4c shows the relationship between the plasmon band shift and reaction time. The effective refractive index (n_{eff}) of the solution is given by $n_{eff} = fn_{react} + (1 - f)n_{prod}$, where n_{react} and n_{prod} are the refractive indexes of the reactant and products, respectively, and f is a fraction of the reactant with respect to the total reagent concentration.[29] Therefore, the plasmon shift can be converted to f or the concentration of lactic acid, [L], by using the sensitivity factor (34.5 nm RIU^{-1}) of the AuPt/CdS hollow cubes. From the point of view of the reaction kinetics, lactic acid decomposition is a first-order reaction. If we suggest that the hydrogen generated from the reaction is in a gaseous state,[30] the hydrogen gas hinders the diffusion of the reactants on the active Pt sites and subsequently slows the reaction rate. This effect is reflected by the kinetic equation assuming that the hindrance of the active sites is commensurate with the

hydrogen gas concentration. The observed reaction rate, k_{obs}, is then corrected to be $\{(A - ax)/A\}\cdot k$, where A is the pre-exponential Arrhenius factor, a is the site hindrance factor by hydrogen gas, x is the hydrogen gas concentration, and k is the actual reaction rate on the Pt sites. It is noted that A is a measure of the rate at which collisions occur irrespective of the particles' energy. The solution to the first-order kinetic equation with the site hindrance factor is (Supporting Information, illustration S1):

$$\frac{x_{sat}}{x_{sat} - [L]_0}\ln\left(\frac{x_{sat} - x}{x_{sat}}\frac{[L]_0}{[L]_0 - x}\right) = kt \quad (1)$$

where $[L]_0$ is the original concentration of lactic acid, x is the hydrogen concentration, and x_{sat} is the hydrogen concentration at the saturation state. The experimental data are plotted on the basis of this equation (Figure 4c, inset), and k is estimated to be 5.3×10^{-6} M^{-1} s^{-1} using a least-squares regression.

Figure 4d is a graph of the change in the extinction peak during the reaction time for a single Au@Pt/CdS cube. The $\Delta\lambda_{max}$ is −4.6 nm, which is nearly one-third of the value of the AuPt/CdS hollow cube. This is because the Au core is, on average, 20 nm removed from the active Pt sites on the hollow shell; thus, the surroundings around the Au core are not completely filled with hydrogen gas even in the saturation state. The kinetic analysis estimates k to be 2.6×10^{-6} M^{-1} s^{-1} (Figure 4e, inset). It is interesting that the peak shift is delayed for 3 min after the reaction starts (Figure 3e), which is also due to the distance between the Au probe and the actual reaction site (vide infra).

Ten individual particles for both catalyst structures were investigated by dark-field spectroscopy (Table 1). Figure 5a
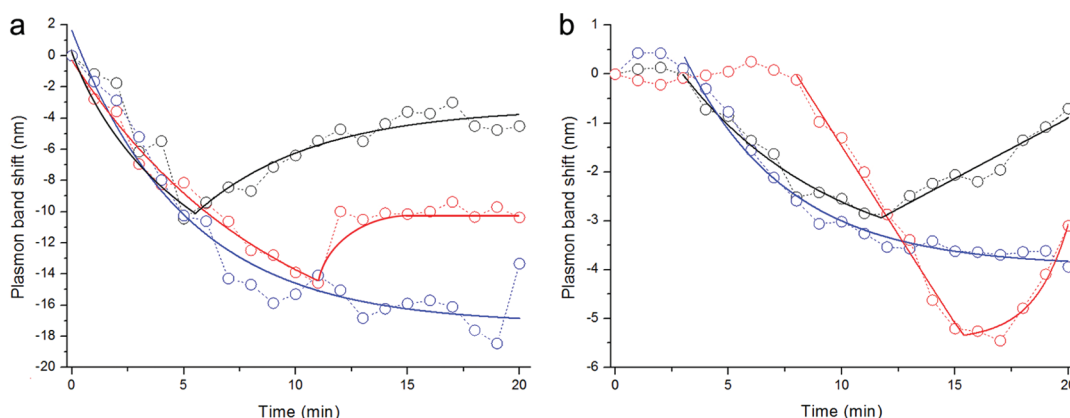
Figure 5. Reaction behaviors of individual catalyst particles. Plasmon band shifts along the reaction progress for three individual (a) AuPt/CdS hollow cubes and (b) Au@Pt/CdS cubes, respectively.

shows the plasmon band shifts of three characteristic particles during the reaction for the AuPt/CdS hollow cubes. All particles exhibit plasmon band shifts to shorter wavelengths. A kinetic analysis of the peak shifts using eq 1 estimates the average k to be $(9.5 \pm 4.5) \times 10^{-6}$ M^{-1} min^{-1} (Table 1a), which is reasonable considering the structural and compositional variations of the catalyst particles. At the initial state of the reaction when t approaches zero, hydrogen molecules are generated at an average rate of 5.7×10^{-17} mL min^{-1} or 1500 molecules per minute on a single catalyst particle. For the individual Au@Pt/CdS cubes, the average rate constant is estimated to be $(6.5 \pm 3.2) \times 10^{-6}$ M^{-1} min^{-1}, and the average rate of hydrogen generation at the initial state is 5.1×10^{-17} mL min^{-1} or 1300 molecules per minute on a single particle (Figure 5b and Table 1b).

As shown in Figure 5a and b, some particles exhibit interesting reverse red-shifts of the extinction peaks at certain times during the reaction. These red-shifts are attributed to the fact that the internal pressure of the hollow cube continuously increases due to hydrogen gas generation when the pore density of the hollow shell is not sufficient to release the pressure. At a certain time, the hydrogen gas begins to leak out through the shell, and the solution diffuses back into the internal vacancy to reach the equilibrium state. The diffusion coefficient (D) of the hollow cube is derived from $D = \pi\chi^2/4t$, where χ is the average diffusion distance of the solution and t is the period to close the equilibrium state. Haes et al. reported that the plasmon shift was linearly proportional to the thicknesses of the self-assembled monolayers on Au and Ag nanoparticles within a distance of 15 nm and was nearly saturated above this range.[31] If we regard this value as the effective plasmon shift distance for one of the single AuPt/CdS hollow cubes (red in Figure 4a), χ can be derived using the ratio of the reverse red-shift (5.2 nm) by back-diffusion of the solution and the maximum blue-shift (-14.6 nm) by hydrogen gas generation. The resultant diffusion coefficient through the shell is estimated to be 3.7×10^{-19} m^2 s^{-1}, which is comparable to coefficients of silica[32] and polymer hollow nanoparticles.[33] The other catalyst particle (black in Figure 5a) has a diffusion coefficient of 1.2×10^{-19} m^2 s^{-1}. For the Au@Pt/CdS cube, the diffusion coefficients of the two individual particles (red and black in Figure 4b) are estimated to be 1.8×10^{-19} and 2.1×10^{-19} m^2 s^{-1}. Thirteen out of 20 particles did not exhibit such reversal red-shifts of the plasmon bands, because of large

defects or sufficiently high pore density in their hollow shells (Table 1, Supporting Information, Figures S14, S15).

Another noticeable feature is that the Au@Pt/CdS cubes show an initial delay time in the plasmon band shift with particle-to-particle variation, whereas the AuPt/CdS hollow cubes do not. When the active Pt site is far from the Au probe as in the Au@Pt/CdS cube, it takes some time for the hydrogen gas evolved at the active sites to reach the effective detection range from the Au core. Using the initial reaction rate and the delay time of each catalyst particle, the distance (d) between the Pt site and the Au probe can be calculated. For the three particles in Figure 5b, the distances are estimated to be 25.3 (red), 17.2 (black), and 16.9 nm (blue), respectively. The total average distance for 10 particles is 20.3 nm, which exactly matches the average distance (20 nm) between the Pt/CdS shells and the Au cores measured from the SEM images (Table 1b). This confirms that the maximum detection range of the plasmon band shift, 15 nm, is a reasonable value in our measurements.

■ CONCLUSIONS

In summary, a rational design of Pt/CdS catalysts with Au probes enables us to monitor the hydrogen generation reaction in situ at the single-particle level by dark-field spectroscopy. The plasmon band shifts of the Au probes show significant particle-to-particle variation, and kinetic analyses provide accurate information regarding the rate constant (k), diffusion coefficient (D), and average distance (d) between the active sites and the probe of individual catalyst particles. This strategy is versatile and can be applied to various reactions that feature large refractive index differences between the reactants and products. Optimization of the measurement using a laser light source would allow the monitoring of fast reactions with extremely high sensitivity up to the molecular level.

■ ASSOCIATED CONTENT

Ⓢ Supporting Information

Additional figures of characterization data and reaction profiles for individual catalyst particles. This material is available free of charge via the Internet at http://pubs.acs.org.

■ AUTHOR INFORMATION

Corresponding Author

hsong@kaist.ac.kr

■ REFERENCES

(1) Turner, M.; Golovko, V. B.; Vaughan, O. P. H.; Abdulkin, P.; Berenguer-Murcia, A.; Tikhov, M. S.; Johnson, B. F. G. *Nature* **2008**, *454*, 981−984.

(2) Herzing, A. A.; Kiely, C. J.; Carley, A. F.; Landon, P.; Hutchings, G. J. *Science* **2008**, *321*, 1331−1335.

(3) Li, Y.; El-Sayed, M. A. *J. Phys. Chem. B* **2001**, *105*, 8938−8943.

(4) Narayanan, R.; El-Sayed, M. A. *Nano Lett.* **2004**, *4*, 1343−1348.

(5) Park, I.; Lee, K.; Choi, J.; Park, H.; Sung, Y. *J. Phys. Chem. C* **2007**, *111*, 19126−19133.

(6) Chen, X.; Moskovits, M. *Nano Lett.* **2007**, *7*, 807−812.

(7) Baldauf, M.; Kolb, D. M. *J. Phys. Chem.* **1996**, *100*, 11375−11381.

(8) Ertl, G. *Angew. Chem., Int. Ed.* **2008**, *47*, 3524−3535.

(9) Somorjai, G. A.; Park, J. Y. *Catal. Lett.* **2007**, *115*, 87−98.

(10) Goodman, D. W. *Chem. Rev.* **1995**, *95*, 523−536.

(11) Habas, S. E.; Lee, H.; Radmilovic, V.; Somojai, G. A.; Yang, P. *Nat. Mater.* **2007**, *6*, 692−697.

(12) Haes, A. J.; Zou, S.; Schatz, G. C.; Van Duyne, R. P. *J. Phys. Chem. B* **2004**, *108*, 6961−6968.

(13) Anker, J. N.; Hall, W. P.; Lyandres, O.; Shah, N. C.; Zhao, J.; Van Duyne, R. P. *Nat. Mater.* **2008**, *7*, 442−453.

(14) Larsson, E. M.; Langhammer, C.; Zoric, I.; Kasemo, B. *Science* **2009**, *326*, 1091−1094.

(15) Novo, C.; Funston, A. M.; Mulvaney, P. *Nat. Nanotechnol.* **2008**, *3*, 598−602.

(16) Xu, W.; Kong, J. S.; Yeh, Y.-T. E.; Chen, P. *Nat. Mater.* **2008**, *7*, 992−996.

(17) Novo, C.; Funston, A. M.; Gooding, A. K.; Mulvaney, P. *J. Am. Chem. Soc.* **2009**, *131*, 14664−14666.

(18) Liu, N.; Tang, M. L.; Hentschel, M.; Giessen, H.; Alivisatos, A. P. *Nat. Mater.* **2011**, *10*, 631−636.

(19) Tang, M. L.; Liu, N.; Dionne, J. A.; Alivisatos, A. P. *J. Am. Chem. Soc.* **2011**, *133*, 13220−13223.

(20) Zhang, Q.; Li, W.; Wen, L.-P.; Chen, J.; Xia, Y. *Chem.-Eur. J.* **2010**, *16*, 10234−10239.

(21) Park, G.; Seo, D.; Jung, J.; Ryu, S.; Song, H. *J. Phys. Chem. C* **2011**, *115*, 9417−9423.

(22) Harada, H.; Ueta, T.; Sakata, T. *J. Phys. Chem.* **1989**, *93*, 1542−1548.

(23) Wark, S. E.; Hsia, C.-H.; Son, D. H. *J. Am. Chem. Soc.* **2008**, *130*, 9550−9555.

(24) Allen, R. L.; Moore, W. J. *J. Phys. Chem.* **1959**, *63*, 223−226.

(25) Prodan, E.; Radloff, C.; Halas, N. J.; Nordlander, P. *Science* **2003**, *17*, 419−422.

(26) Sheikholeslami, S.; Jun, Y.-w.; Jain, P. K.; Alivisatos, A. P. *Nano Lett.* **2010**, *10*, 2655−2660.

(27) Sun, Y.; Mayers, B.; Xia, Y. *Adv. Mater.* **2003**, *15*, 641−646.

(28) Mulvaney, P. *Langmuir* **1996**, *12*, 788−800.

(29) Novo, C.; Funston, A. M.; Pastoriza-Santos, I.; Liz-Marzan, L. M.; Mulvaney, P. *J. Phys. Chem. C* **2008**, *112*, 3−7.

(30) Holmberg, M.; Kuhle, A.; Garnaes, J.; Morch, K. A.; Boisen, A. *Langmuir* **2003**, *19*, 10510−10513.

(31) Haes, A. J.; Zou, S.; Schatz, G. C.; Van Duyne, R. P. *J. Phys. Chem. B* **2004**, *108*, 109−116.

(32) Lee, J.; Park, J. C.; Song, H. *Adv. Mater.* **2008**, *20*, 1523−1528.

(33) Kamata, K.; Lu, Y.; Xia, Y. *J. Am. Chem. Soc.* **2003**, *125*, 2384−2385.